



On the frequency-dependent complex-dielectric, complex-electric modulus and conductivity in Au/(NiS:PVP)/*n*-Si structures

Ş. Altındal^{1,*}, M. Ulusoy^{1,*} , S. Özçelik^{2,3}, and Y. Azizian-Kalandaragh^{2,3}

¹Department of Physics, Faculty of Sciences, Gazi University, Ankara, Turkey

²Photonics Application and Research Center, Gazi University, 06500 Ankara, Turkey

³Photonics Department, Applied Science Faculty, Gazi University, 06500 Ankara, Turkey

Received: 13 April 2021

Accepted: 15 June 2021

Published online:
17 July 2021

© Springer Science+Business
Media, LLC, part of Springer
Nature 2021

ABSTRACT

The values of complex-dielectric ($\varepsilon^* = \varepsilon' - j\varepsilon''$), loss-tangent ($\tan\delta$), complex-electric modulus ($M^* = M' + jM''$), and ac electrical-conductivity (σ_{ac}) of the performed Au/(NiS:PVP)/*n*-Si structures were extracted from the measured impedance-spectroscopy method (ISM) in frequency range of 10 kHz–1 MHz and voltage ((− 2 V)–(+ 3 V)). These parameters, which constitute the main subject of our study, have been obtained from high frequency and voltage values, more particularly in the depletion and accumulation regions. The decrease of dielectric-constant (ε'), dielectric-loss (ε''), and $\tan\delta$ with increasing frequency for almost every voltage were explained by Maxwell–Wagner type relaxation processes. The observed higher-values of ε' and ε'' at low frequencies result from surface-states (N_{ss}) and dipole-polarization. Since N_{ss} has sufficient time to keep up with the applied voltage signal, dipoles can respond to the electric field to reorient themselves. An increase in M' values was observed at increasing frequency values attributed to the long-distance mobility of the carriers. On the other hand, the observed peak in the $M'' - \ln(f)$ curves was attributed to a distinctive distribution of N_{ss} located at Au/(NiS:PVP) interface depend on their lifetime. The obtained value of ε' even at 10 kHz at 3 V is indicated that the used (NiS:PVP) organic-interlayer can be used a superior alternative instead of SiO₂ or SnO₂ which are conventional interlayers thanks to its low-cost, flexibility, easy production techniques such as spin-coating or electro-spinning technique at room condition, successfully.

Address correspondence to E-mail: altundal@gazi.edu.tr; ulusoymurat@gazi.edu.tr

1 Introduction

For determination of the performance of the metal–semiconductor (MS) structures with a thin film such as polymer and ferroelectric interfacial layer (MPS and MFS) well, it depends on a detailed study of their both electrical and dielectric features in a wide range of voltage and frequency as well as temperature [1–5]. At the same time, their performance depends on many factors such as doping level of donor/acceptor atoms, interlayer thickness and permittivity, barrier-inhomogeneities at MS contact region, fabrication processes, the existence of series-resistance (R_s) and N_{ss} [6–11]. From the equation of $C = \epsilon' \epsilon_0 A / d$, it is obvious that for changing the value of C we need to increase of ϵ' and decrease of interface layer thickness (d). But it is known that the value of thickness is obtained by the working voltage and cannot be adjusted. Accordingly, an organic interlayer with high dielectric constant such as a polymer interlayer can be used to increase the C value of MIS or MPS structures because the C value is considerably dependent on the dielectric constant (ϵ') [1].

Recently, organic polymers such as polyvinylpyrrolidone (PVP) and PVA with and without metal or metal-oxide/sulfide doped at MS interface thanks to high dielectric constant have become very interesting for the researchers. In addition to this, the preparation of MPS type structures has significant advantages thanks to their low cost, flexibility, mechanical strength, easy grown techniques in room condition such as spin-coating, electro-spinning, and sol–gel [12–18]. However, the polarization process in high-dielectric materials occurs easily when an external electric field is applied, and it influences the position of the traps and ions. [19]. On the other hand, electronic and ionic polarizations may be dominated at higher frequency values (10^{10} – 10^{15} Hz), but surface and dipole polarizations may be dominated at the frequency range of 1 kHz–1 MHz or few kHz, respectively [20–22]. These changes observed at significantly low and medium frequencies can be explained by the relaxation phenomena. Accordingly, the interfacial electric dipoles have sufficient time to align with the electric field before changing the field direction. That is, dipoles at the interface can keep up with the electric field changing, and consequently, the value of the dielectric constant increases significantly with

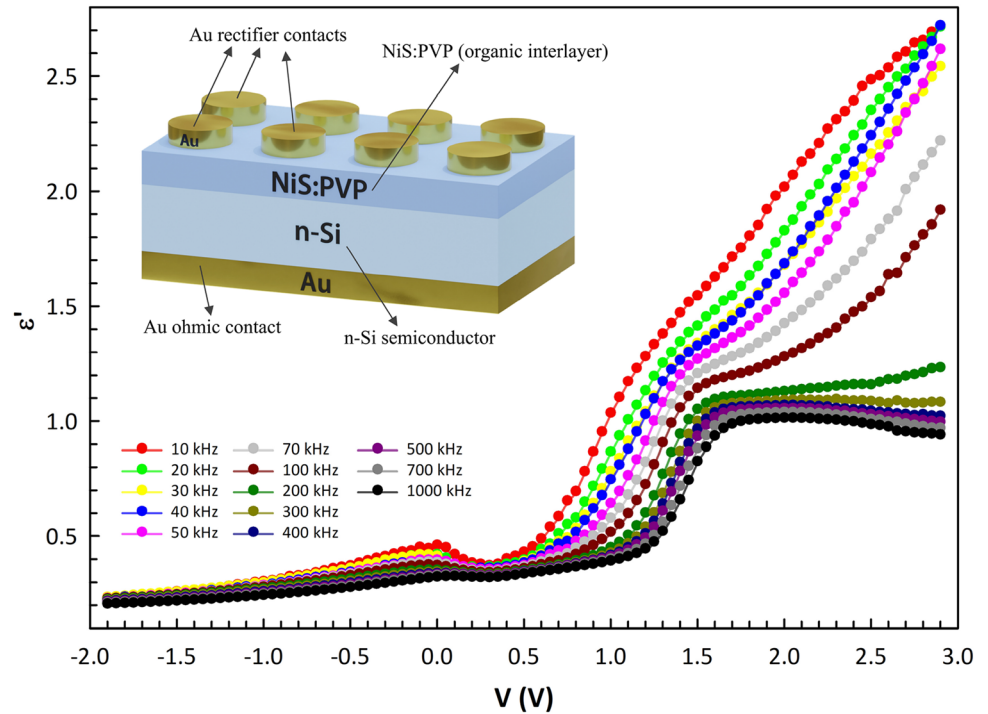
decreasing frequency. On the contrary, at higher frequencies, since the electric field change is too fast, the dipoles cannot align with the field direction as a result of shorter time, and hence the value of the dielectric constant decreases [23, 24]. Therefore, the investigation of dielectric features of the MPS type structures is of great importance to achieve much more understanding of the conduction mechanism and polarization processes. In this study, considering the above-said situations σ_{ac} , M^* , $\tan\delta$ and dielectric features of the Au/(NiS: PVP)/ n -Si structure whose schematic structure were illustrated inset in Fig. 1 have been examined in detail and presented depending on the different frequencies and varying-voltage ranges.

In our previous study [25], the fundamental electrical parameters of the fabricated Au/(NiS:PVP)/ n -Si structures were derived from the slope and intercept linear parts of the reverse bias C^{-2} vs V curves as a function of frequency, and they found the strong frequency function. In addition, the density of energy distribution of N_{ss} and the series resistance (R_s) were obtained from the Admittance and Conductance methods, respectively. Here, we aimed that the investigate frequency and voltage-dependent profiles of ϵ' , ϵ'' , $\tan\delta$, M' , M'' , and σ_{ac} of these structures in detail as the second part of our previous study. The observed higher-values of ϵ' and ϵ'' at low-frequencies are results of surface-states (N_{ss}) and dipole-polarization. Because N_{ss} have sufficient time to keep up with the ac-signal changing easily, dipoles can react to the electric field to reorient themselves. The above-said parameters were also observed as a strong function of frequency and voltage both at the depletion and accumulation regions. While the changes in these parameters in depletion layer were attributed to a distinctive distribution of N_{ss} located at Au/(NiS:PVP) interlayer depend on their life-time and polarization, the changes at the accumulation region were attributed to the R_s and organic interlayer.

2 Experimental details

The Au/(NiS-PVP)/ n -Si structures were manufactured on the n -Si substrate with Phosphorus-doped, 300 μm thickness, 5.08 cm diameter, 4 Ω cm, and one-side polished. In the first step, n -Si wafer was cleaned in the H_2O , H_2O_2 , and NH_4OH (3:1:1) chemical solution at about 70 $^\circ\text{C}$ in the ultrasonic-bath for

Fig. 1 The ϵ' vs V curves of the Au/(NiS:PVP)/ n -Si structure for different frequencies and inset the structural architecture of the Au/(NiS:PVP)/ n -Si



5 min and subsequently rinsed in the high-resistivity deionized-water (DW) at 10 min. Secondly, all back of the wafer was coated by Au with high-pure (99.999%) and 150 nm by using thermally evaporation system at 10^{-6} Torr and then to form a good ohmic contact, and it was annealed at 500 °C in the nitrogen-ambient for 5 min. In the third step, the solution (NiS-PVP) was coated on the front of n -Si wafer by means of spin-coating method (SCM) due to its higher spin-velocity and longer spin-times leads to create a thinner film on the n -Si wafer. High-pure NiS was purchased from Sigma-Aldrich company, and it was dissolved in DW. Finally, circular Au dots or rectifier-contacts with 1 mm diameter and 150 nm thickness were also evaporated onto the (NiS-PVP) interlayer at 10^{-6} Torr. For a representation the schematic diagram of Au/(NiS:PVP)/ n -Si structures, the measured system, and experimental setup can be seen in the preceding study [25]. The frequency-dependent values of the real and imaginary part of the dielectric constant were obtained from measured capacitance/conductance–voltage (C/G - V) curves in the frequency range of 10 kHz–1 MHz and (– 2 V)–(+ 3 V) which are executed by means of a micro-computer an IEEE-488 ac/dc converter card by using HP4192A LF impedance meter.

3 Results and discussion

The dielectric constant and dielectric loss of the interlayer, in which the energies are stored and released by the interface states in each oscillation of the ac signal applied to the structure, are defined as the real (ϵ') and imaginary (ϵ'') components of the complex dielectric constant (ϵ^*). For this reason, the dependence of ϵ' and ϵ'' on voltage were obtained from the measured voltage-dependent profile of the C - V and G/ω - V curves from – 2 to + 3 V with 0.05 V steps by using Eq. 1. Thus, the obtained ϵ' - V and ϵ'' - V curves of the Au/(NiS:PVP)/ n -Si structure were shown in Figs. 1 and 2 in the frequencies between 10 kHz and 1 MHz, respectively.

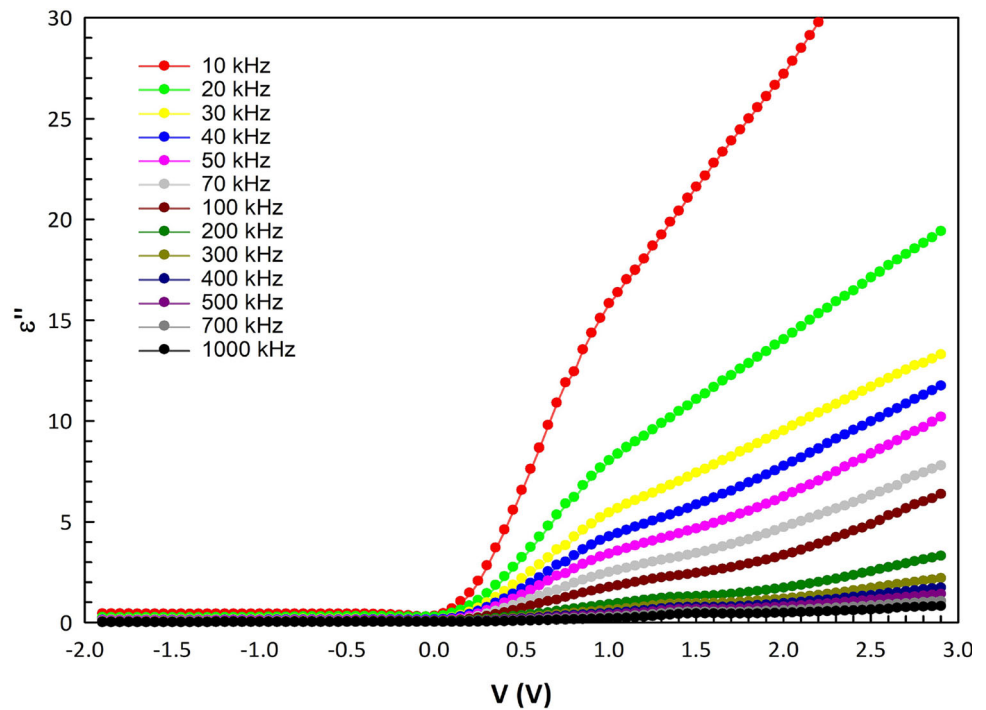
It is obviously seen that in Figs. 1 and 2, both the ϵ' - V and ϵ'' - V curves have typical MOS or MIS type capacitors characteristics with regions of accumulation, depletion, and inversion zone, especially for enough high frequencies ($f \geq 100$ kHz).

$$\epsilon^*(\omega) = \epsilon' - j\epsilon'' = C_m/C_0 - j(G_m/\omega C_0) \quad \text{with} \quad (1)$$

$$C_0 = \epsilon_0 A/\delta_i$$

In Eq. 1; the quantities of ω , C_m , G_m , C_0 , and d_i are the angular frequency, measured capacitance and conductance at any bias voltage, the empty capacitance (constant) and interlayer thickness, respectively. The value of dielectric-loss tangent ($\tan\delta$) for

Fig. 2 The ϵ'' vs V curves of the Au/(NiS:PVP)/ n -Si structure for different frequencies

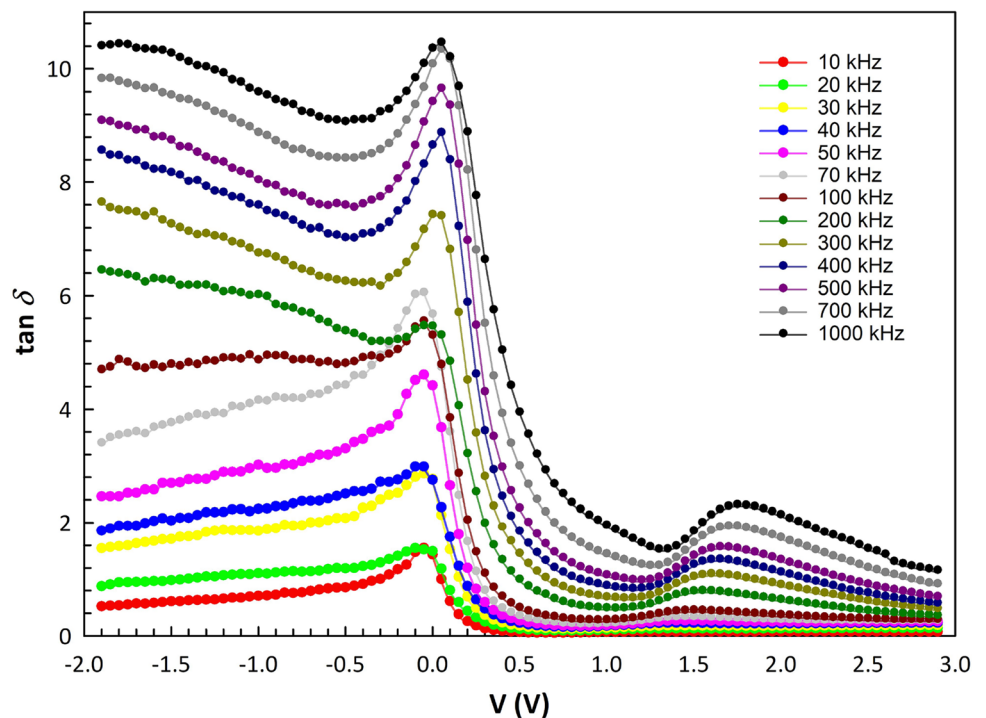


an interlayer is usually described the dielectric loss divided by dielectric constant as given follow [21–24]:

$$\tan(\delta) = \frac{\epsilon''}{\epsilon'} \quad (2)$$

Thus, the dependence of $\tan\delta$ on voltage was obtained from Eq. 2 and represented in Fig. 3. As illustrated in Fig. 3, $(\tan\delta)$ – V curves have two distinctive peaks at low/moderate frequencies which are positioned at nearly 0 V and 1.8 V as a

Fig. 3 The $\tan(\delta)$ vs V curves of the Au/(NiS:PVP)/ n -Si structure for different frequencies



consequence of the distinctive distribution of surface states and R_s , respectively.

The observed changes both in the value of ϵ' and ϵ'' with frequency in the depletion region are result from the existence of the surface states (N_{ss}) between (NiS:PVP) interlayer and Si and their life-time (τ) and interfacial or dipole polarization. Surface-states are usually originated from semiconductor-surface imperfection, oxygen-vacancies, structural rearrangements due to metallization, doping level of donor/acceptor atoms and interfacial layer at M/S interface. These traps or states are considerably effective on the electrical parameters and conduction mechanism of the fabricated semiconductor devices. According to Card and Rhoderick, they can be also considered as electronic states generated by unsaturated dangling-bonds of the surface atoms and some organic-contaminations in laboratory-environment [1, 2]. Because, during the elaboration of semiconductor devices such as MS or MIS type structures, many surface-states can be occurred which they lead to electronic states with energies located in the band gap of semiconductor at interlayer/semiconductor interface as randomly. Such non-homogeneity of them sometimes is called as “a special density distribution”.

The dipole and interfacial type polarization is known as Maxwell–Wagner type polarization [12, 23, 24]. Because, at low frequencies, electrons which are positioned at surface states have sufficient time to keep up with the external alternating ac signal, and so they give rise to an increase both in the value of ϵ' and ϵ'' . Similarly, dipoles have enough time to rotate around themselves parallel to the changing electric field direction. But at high frequencies, both the surface states and dipole have not enough time to keep up with ac signal and dipoles, in this case, cannot rotate around themselves rapidly in the applied voltage and thus cannot yield an excessive value to measure of ϵ' and ϵ'' . Therefore, the obtained higher values of them at low/moderate frequencies be able to attribute to the surface/dipole polarization and surface states. The observed splitting in the ϵ' and ϵ'' in the depletion region results from re-structure and re-order charges at traps under the electric field. On the other side, this splitting at the accumulation region results from series resistance (R_s) of the structure at high frequencies. In other words, while N_{ss} are effectual in inversion and depletion regions at moderate or lower frequencies, R_s of the structure is effectual merely at the accumulation region at higher frequencies.

As illustrated in Figs. 1, 2 and 3, the values of ϵ' , ϵ'' , and $\tan\delta$ are considerably changed from electric-field/voltage and frequency, remarkably in depletion and accumulation regions. Therefore, dependence on frequency of these parameters are illustrated in Figs. 4, 5 and 6 for various bias voltages (0.5–3 V by 50 mV steps) to determine changes of them with frequency. Because only at one frequency and under one electric field/voltage C and G/ω measurements cannot supply enough information to us on the conduction mechanisms, polarization or relaxation phenomenon, and surface states.

It can be obviously seen that in these figures (Figs. 4, 5 and 6), all the values of ϵ' , ϵ'' , and $\tan\delta$ decrease with increasing frequency as exponentially for each voltage. Such higher values of ϵ' , ϵ'' , and $\tan\delta$ at moderate or lower frequencies under various bias voltage can be understood concerning charge storage at surface states and the existence of strong surface/interfacial or dipole polarizations at lower frequencies. Because the existence of (NiS:PVP) interlayer between Au and n -Si can be easily polarized under the influence of an external electric field that can remove charges located at the interlayer from their equilibrium locations or traps. The observed a broad peak in the ϵ' vs $\ln(f)$ curves at low frequencies (Fig. 4) and crossing behavior of the $\tan\delta$ vs $\ln(f)$ curves can be attributed to the re-structure and re-order of surface states and dipoles under electric field.

With the aim of obtaining more information on both the electrical-transport mechanisms and relaxation or polarization processes for MIS/MPS type structures, complex electric-modulus ($M^* = 1/\epsilon^*$) can be used as successfully in wide frequency and voltage range. For this aim, using the experimental values of ϵ' (Fig. 1) and ϵ'' (Fig. 2) obtained for each frequency, both the M' and M'' components of M^* versus the applied voltage was calculated with the help of Eq. 3 and so given in Figs. 7 and 8, respectively. [12, 26–30]:

$$M^* = \frac{1}{\epsilon^*} = M' + jM'' = \frac{\epsilon'}{\epsilon'^2 + \epsilon''^2} + j \frac{\epsilon''}{\epsilon'^2 + \epsilon''^2} \quad (3)$$

It is seen that in Figs. 7 and 8, both M' and M'' values usually decline with increasing voltage and give a peak in the depletion region. These declines in M' and M'' with increasing voltage are result from the increasing values of ϵ' (Fig. 1) and ϵ'' (Fig. 2) as shown in Eq. 3. The observed peak in the $M'-V$ and $M''-V$ curves in the depletion region and shift towards the accumulation region of these peaks can be understood from the re-

Fig. 4 The ϵ' vs $\ln(f)$ curves of the Au/(NiS:PVP)/*n*-Si structure for different bias voltages

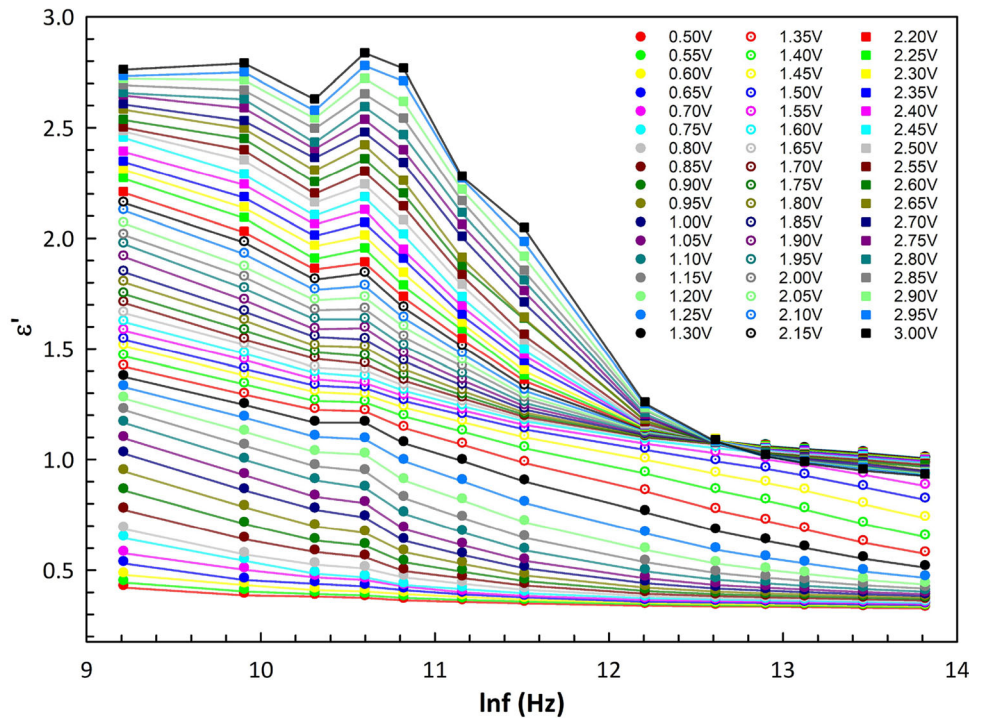
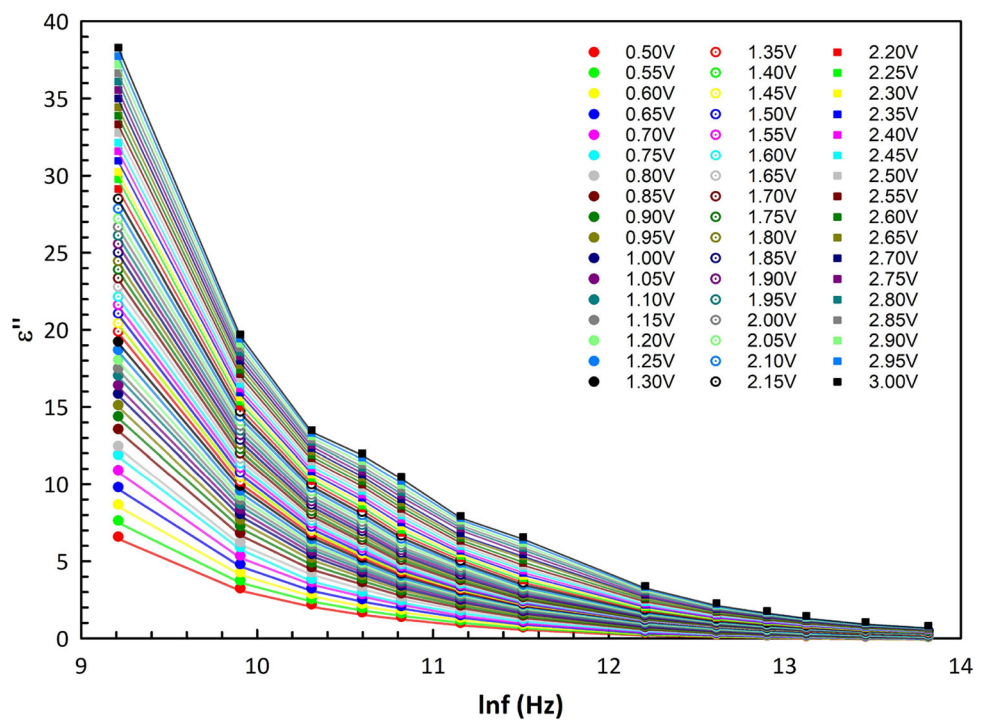


Fig. 5 The ϵ'' vs $\ln(f)$ curves of the Au/(NiS:PVP)/*n*-Si structure for different bias voltages



order and re-structure of charges at surface states, and interfacial/dipole polarization under external electric field depend on period ($T = 1/2\pi f$) and relaxation time of surface state [4, 5, 12, 30]. In order to clearly seen the M' and M'' values depending on the frequency in both the depletion and accumulation region, the

$M' - \ln(f)$ and $M'' - \ln(f)$ curves are also derived from Figs. 7 and 8, and thus the curves are shown in Figs. 9 and 10, respectively.

It can be obviously seen that in Fig. 9, M' values exhibit almost exponential increases with increasing frequency. In other words, the values increasing are

Fig. 6 The double-logarithmic $\tan \delta$ vs f curves of the Au/(NiS:PVP)/ n -Si structure for different bias voltages

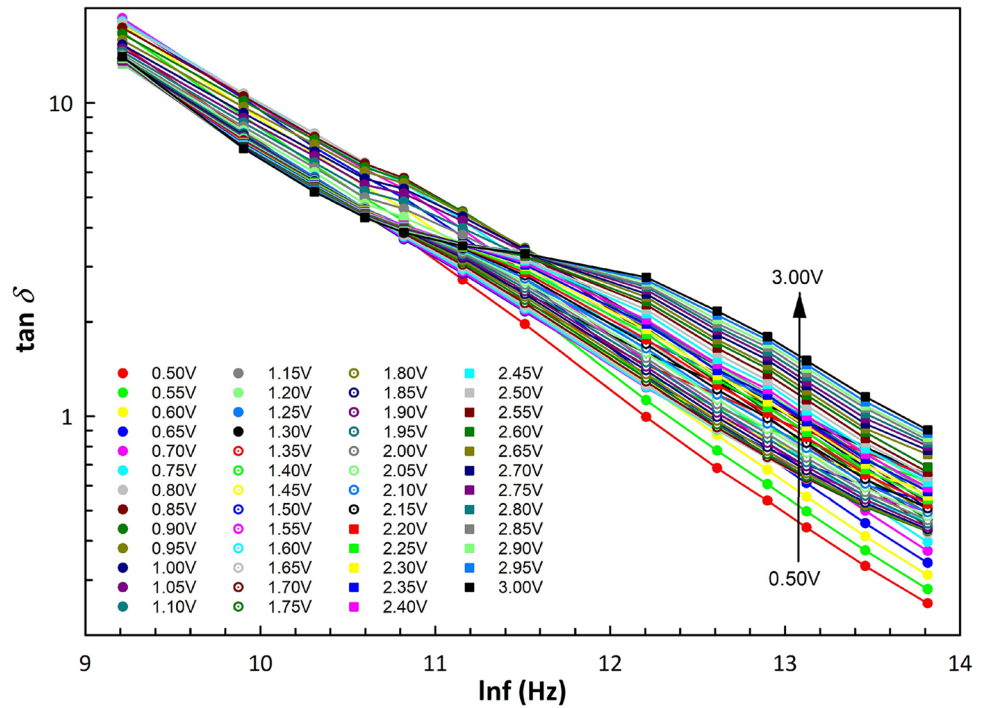
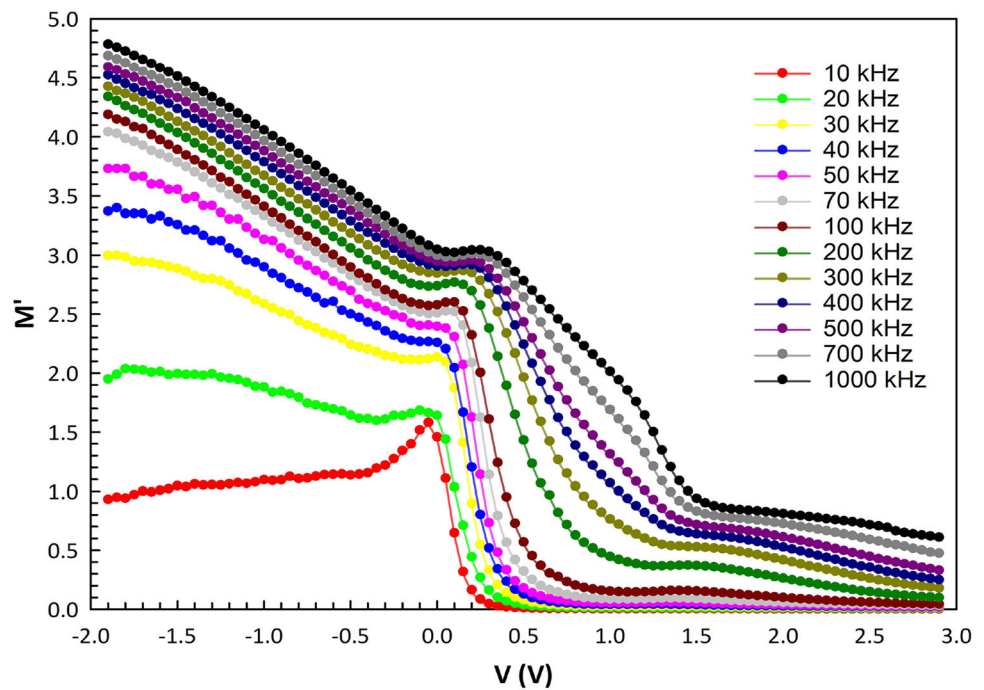


Fig. 7 The M' vs V curves of the Au/(NiS:PVP)/ n -Si structure for different frequencies



almost closer to 0 at lower frequencies as a consequence of the range mobility of charge carriers. On the other side, the $M'' - \ln(f)$ curves have a peak, as can be seen obviously. While the amplitude of the peaks declines with increasing applied bias voltage, the location of the peaks shifts towards higher frequencies. The observed peak in the $M'' - \ln(f)$ curves

is the result of the relaxation process, and this case is defined by $\omega\tau = 1$. The peaks that occurred represent the transition between short and long-distance charge-carrier mobility. As illustrated from Fig. 10, the $M'' - \ln(f)$ curves are indicative of these peaks.

In order to determine the variation in the ac conductivity ($\sigma_{ac} = \epsilon_0 \epsilon'' \omega$), the double-logarithmic σ_{ac} vs

Fig. 8 The M'' vs V curves of the Au/(NiS:PVP)/ n -Si structure for different frequencies and inset of them between 0 and 1.1 V to see the peak behavior as clearly

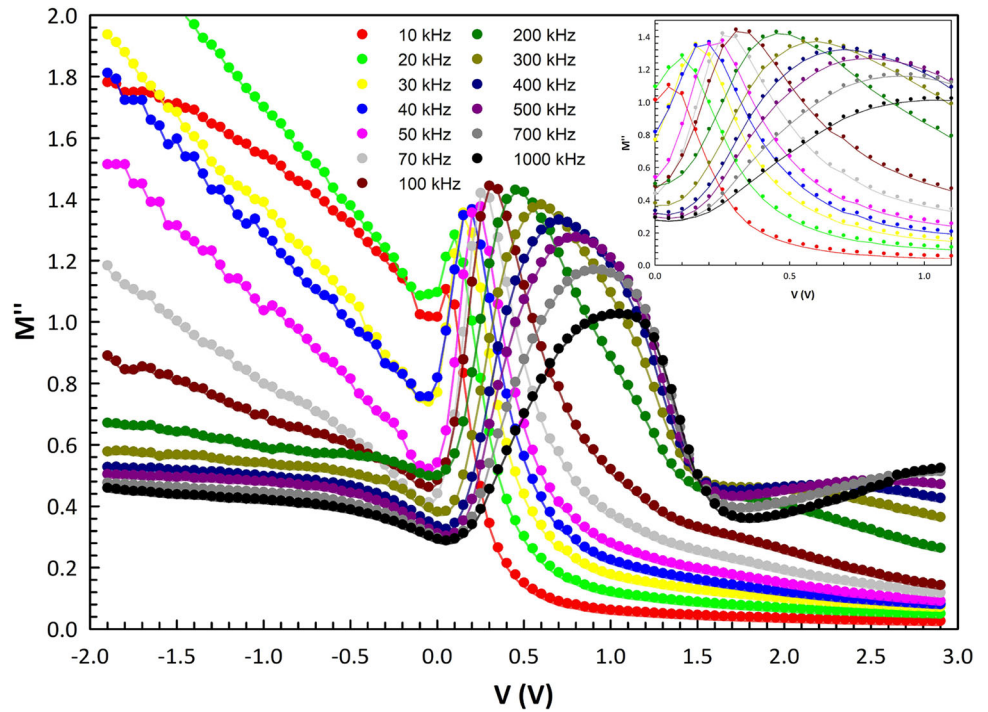
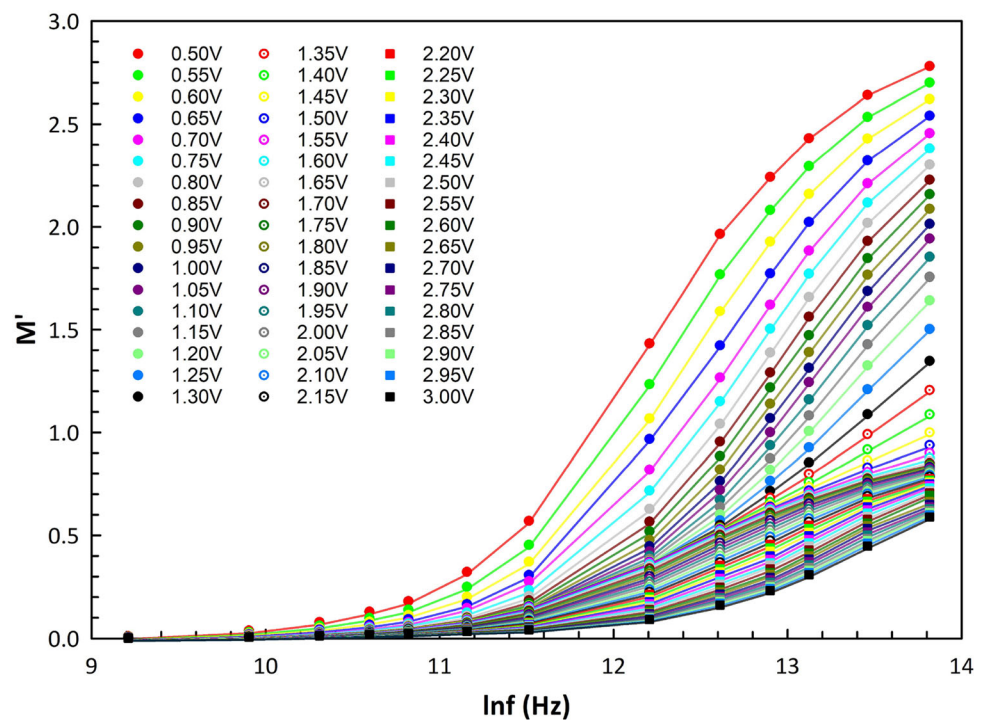


Fig. 9 The M' vs $\ln(f)$ curves of the Au/(NiS:PVP)/ n -Si structure for different bias voltages



f curves for the various bias voltage (1.5–3 V by 50 mV steps) and is illustrated in Fig. 11. According to the figure, the σ_{ac} values increase as the positive voltage range increases (in depletion and accumulation regimes). On the other side, the value of σ_{ac} becomes almost frequency independent at low

frequencies, but it starts to increase at high frequencies. In other words, the lower values of conductivity at low frequencies are defined as dc conductivity. The increase in σ_{ac} at high frequency can be predicated on the hopping conduction of mobile charge carriers. As a result, the value of σ_{ac} is with regard to the

Fig. 10 The M'' vs $\ln(f)$ curves of the Au/(NiS:PVP)/ n -Si structure for different bias voltages and inset of them between 1.55 and 3.00 V to see the peak behavior as clearly

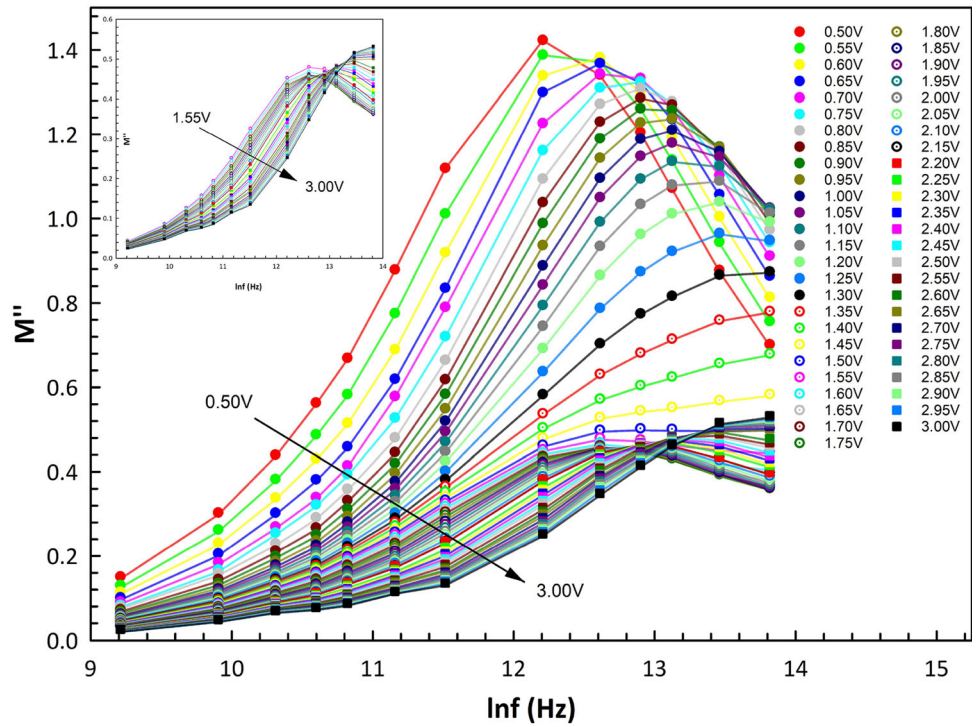
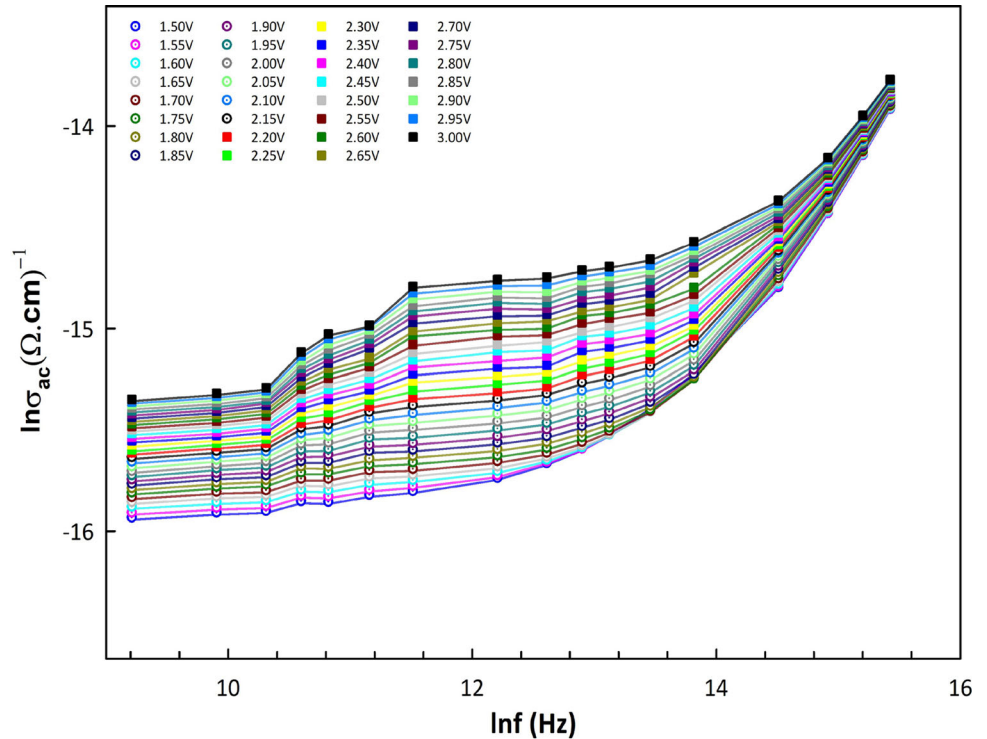


Fig. 11 The double logarithmic σ_{ac} vs f curves of the Au/(NiS:PVP)/ n -Si structure for different bias voltages



dielectric loss (ϵ'') and frequency. The similar results both on dielectric properties/electric modulus, and ac conductivity as function of frequency and applied electric field were reported in the literature in very recently [31–41].

4 Conclusions

In this research paper, the frequency and applied bias voltage dependence of ϵ^* , $\tan\delta$, M^* and σ_{ac} values of the fabricated Au/(NiS-doped PVP)/ n -Si structures

have been investigated in detail in the wide range frequency (10 kHz–1 MHz) and voltage ($-2\text{ V}/+3\text{ V}$) by using the C_m and G_m values at room temperature. According to the experimental results, the basic dielectric parameters, M' , M'' and σ_{ac} were found the strong frequency and voltage functions. These changes in them become more distinctive both in depletion and accumulation regimes which can be explained by Maxwell–Wagner type relaxation processes, surface states, and R_s . The observed higher-values of ϵ' and ϵ'' at lower frequencies can be explained due to the particular distribution of N_{ss} and dipole-polarization because N_{ss} have sufficient time to easily follow an alternating-signal and dipoles respond to the electric field to reorient themselves. On the other hand, the observed increase in the M' with increasing frequency results from long-distance mobility of carriers. The observed peak in the $M'' - \ln(f)$ curves and shifting its position towards the accumulation region was attributed to the re-ordering and re-structure of charges at surface states, and interfacial/dipole polarization under external electric field depends on the period ($T = 1/2\pi f$) and relaxation time of surface states. The obtained high-value of ϵ' ($= 2.8$) even at 10 kHz and 3 V is indicated that the used (NiS-doped PVP) polymer interface layer has considerable advantages over conventional insulators, for instance, low cost, flexibility, easy fabrication such as spin-coating or electro-spinning technique, and considering the advantages it can be successfully used in room conditions rather than conventional insulators such as SiO_2 or SnO_2 .

Acknowledgements

This study was supported by Gazi University Scientific Research Project. (Project Number: GU-BAP.05/2019-26).

References

1. S.M. Sze, K.K. Ng, *Physics of Semiconductor Devices*, 3rd edn. (Wiley, New Jersey, 2007)
2. E.H. Nicollian, J.R. Brews, *MOS (Metal Oxide Semiconductor) Physics and Technology* (Wiley, New York, 1982)
3. Ç. Bilkan, Y. Azizian-Kalandaragh, Ş Altındal, R. Shokrani-Havigh, Frequency and voltage dependence dielectric properties, ac electrical conductivity and electric modulus profiles in $\text{Al}/\text{Co}_3\text{O}_4\text{-PVA}/\text{p-Si}$ structures. *Phys. B* **500**, 154–160 (2016)
4. S. Karadas, S. Altındal Yerişkin, M. Balbaşı, Y. Azizian-Kalandaragh, Complex dielectric, complex electric modulus, and electrical conductivity, in $\text{Al}/(\text{Graphene-PVA})/\text{p-Si}$ (metal-polymer-semiconductor) structures. *J. Phys. Chem. Solids* **148**, 109740 (2021)
5. S. Alptekin, A. Tataroğlu, Ş Altındal, Dielectric modulus and conductivity study of $\text{Au}/\text{PVP}/\text{n-Si}$ (MPS) structure in the wide range of frequency and voltage at room temperature. *J. Mater. Sci.: Mater. Electron.* **30**, 6853–6859 (2019)
6. V. Rajagopal Reddy, C. Venkata Prasad, Surface chemical states, electrical and carrier transport properties of $\text{Au}/\text{ZrO}_2/\text{n-GaN}$ MIS junction with a high-k ZrO_2 as an insulating layer. *Mater. Sci. Eng. B* **231**, 74–80 (2018)
7. M.S.P. Reddy, H.S. Kang, J.H. Lee, V.R. Reddy, J.S. Jang, Electrical properties and the role of inhomogeneities at the polyvinyl alcohol/n-inp schottky barrier interface. *J. Appl. Polym. Sci.* **131**, 39773 (2014)
8. H.C. Card, E.H. Rhoderick, Studies of tunnel MOS diodes I. Interface effects in silicon Schottky diodes. *J. Phys. D* **4**, 1589 (1971)
9. M. Sharma, S.K. Tripathi, Frequency and voltage dependence of admittance characteristics of $\text{Al}/\text{Al}_2\text{O}_3/\text{PVA}:\text{n-ZnSe}$ Schottky barrier diodes. *Mater. Sci. Semicond. Process.* **41**, 155–161 (2016)
10. B.L. Sharma, *Metal-Semiconductor Schottky Barrier Junctions and Their Applications* (Plenum Press, New York, 1984)
11. P. Chattopadhyay, The effect of shunt resistance on the electrical characteristics of Schottky barrier diodes. *J. Phys. Appl. Phys.* **29**, 823–829 (1996)
12. A.M. Akbaş, A. Tataroğlu, Ş Altındal, Y. Azizian-Kalandaragh, Frequency dependence of the dielectric properties of $\text{Au}/(\text{NG}:\text{PVP})/\text{n-Si}$ structures. *J. Mater. Sci.: Mater. Electron.* **32**, 7657–7670 (2021)
13. Ö. Sevgili, İ Taşcıoğlu, S. Boughdachi, Y. Azizian-Kalandaragh, Ş Altındal, Examination of dielectric response of $\text{Au}/\text{HgS-PVA}/\text{n-Si}$ (MPS) structure by impedance spectroscopy method. *Phys. B* **566**, 125–135 (2019)
14. C.V. Subba Reddy, X. Han, Q.-Y. Zhu, L.-Q. Mai, W. Chen, Dielectric spectroscopy studies on (PVP+PVA) polyblend film. *Microelectron. Eng.* **83**, 281–285 (2006)
15. Y. Azizian-Kalandaragh, İ Yücedağ, G. Ersöz Demir, Ş Altındal, Investigation of the variation of dielectric properties by applying frequency and voltage to $\text{Al}/(\text{CdS-PVA})/\text{p-Si}$ structures. *J. Mol. Struct.* **1224**, 129325 (2021)
16. S. Altındal Yerişkin, M. Balbaşı, A. Tataroğlu, Frequency and voltage dependence of dielectric properties, complex electric modulus, and electrical conductivity in $\text{Au}/7\%$ graphene

- doped-PVA/n-Si (MPS) structures. *J. Appl. Polym. Sci.* **133**(33), 43827 (2016)
17. N. Karaođlan, H. uslu Tecimer, Ő Altındal, C. Bindal, Dielectric characterization of BSA doped-PANİ interlayered metal-semiconductor structures. *J. Mater. Sci.: Mater. Electron.* **30**, 14224–14232 (2019)
 18. H.G. Çetinkaya, Frequency and voltage dependent profile of dielectric parameters and electric modulus for Al/(HgS-PVA)/p-Si capacitor via impedance Spectroscopy method. *J. Nanoelectron. Optoelectron.* **13**, 421–427 (2018)
 19. L.L. Hench, J.L. West, *Principles of Electronic Cremaics* (Willey, New York, 1990)
 20. M. Mümtaz, N.A. Khan, Dielectric properties of $\text{Cu}_{0.5}\text{Tl}_{0.5}\text{Ba}_2\text{Ca}_3\text{Cu}_4\text{O}_{12-8}$ bulk superconductor. *Phys. C* **469**(13), 728–731 (2009)
 21. C.P. Symth, *Dielectric Behaviour and Structure* (McGraw-Hill, New York, 1995)
 22. A. Chelkowski, *Dielectric Physics* (Elsevier, Amsterdam, 1980)
 23. H.N. Chandrakala, B. Ramaraj, Shivakumaraiah, G.M. Madhu, Siddaramaiah, The influence of zinc oxide–cerium oxide nanoparticles on the structural characteristics and electrical properties of polyvinyl alcohol films. *J. Mater. Sci.: Mater. Electron.* **47**, 8076–8084 (2012)
 24. A. Kyritsis, P. Pissis, J. Grammatikakis, Dielectric relaxation spectroscopy in poly (hydroxyethyl acrylates)/water hydrogels. *J. Polym. Sci. B* **33**, 1737–1750 (1995)
 25. M. Ulusoy, Ő Altındal, P. Durmuş, S. Özçelik, Y. Azizian-Kalandaragh, Frequency and voltage-dependent electrical parameters, interface traps, and series resistance profile of Au/(NiS: PVP)/n-Si structures. *J. Mater. Sci.: Mater. Electron.* **32**, 13693–13707 (2021)
 26. N. Rajeswari, S. Selvasekarapandian, S. Karthikeyan, M. Prabu, G. Hirankumar, H. Nithya, C. Sanjeeviraja, Conductivity and dielectric properties of polyvinyl alcohol–polyvinylpyrrolidone poly blend film using non-aqueous medium. *J. Non-Cryst. Solids* **357**, 3751–3756 (2011)
 27. P.B. Macedo, C.T. Moynihan, R. Bose, The role of ionic diffusion in polarisation in vitreous ionic conductors. *Phys. Chem. Glasses* **13**, 171–179 (1972)
 28. N.G. McCrum, B.E. Read, G. Williams, *Anelastic and Dielectric Effects in Polymeric Solids* (Wiley, London, 1967)
 29. A.A. Sattar, S.A. Rahman, Dielectric properties of rare earth substituted Cu-Zn ferrites. *Phys. Status Solidi* **200**(2), 415–422 (2003)
 30. Y.Ş Asar, T. Asar, Ő Altındal, Investigation of dielectric relaxation and ac electrical conductivity using impedance spectroscopy method in (AuZn)/TiO₂/p-GaAs (110) Schottky barrier diodes. *J. Alloys Compd.* **628**, 442–449 (2015)
 31. İ Taşçıođlu, Ö. Sevgili, Y. Azizian-Kalandaragh, Ő Altındal, Frequency-dependent admittance analysis of Au/n-Si structure with CoSO₄-PVP interfacial layer. *J. Electron. Mater.* **49**, 3720–3727 (2020)
 32. İ Taşçıođlu, S.O. Tan, Ő Altındal, Frequency, voltage and illumination interaction with the electrical characteristic of the CdZnO interlayered Schottky structure. *J. Mater. Sci.: Mater. Electron.* **30**, 11536–11541 (2019)
 33. Ö. Sevgili, İ Taşçıođlu, S. Boughdachi, Y. Azizian-Kalandaragh, Ő Altındal, Examination of dielectric response of Au/HgS-PVA/n-Si (MPS) structure by impedance spectroscopy method. *Phys. B* **566**, 125–135 (2019)
 34. H. Tecimer, On the frequency–voltage dependent electrical and dielectric profiles of the Al/(Zn-PVA)/p-Si structures. *J. Mater. Sci.: Mater. Electron.* **29**, 20141–20145 (2018)
 35. E. Arslan, Y. Asar, İ Taşçıođlu, H. Uslu, E. Özbay, Frequency and temperature dependence of the dielectric and AC electrical conductivity in (Ni/Au)/AlGaIn/AlIn/GaN heterostructures. *Microelectron. Eng.* **87**, 1997–2001 (2010)
 36. T. Tunç, H. Uslu, Ő Altındal, Preparation and dielectric properties of polyvinyl alcohol (Co, Zn Acetate) Fiber/n-Si and polyvinyl alcohol (Ni, Zn Acetate)/n-Si Schottky diodes. *Fibers Polym.* **12**, 886 (2011)
 37. S.O. Tan, Identification of the frequency- and voltage-dependent dielectric characterization of metal-Zn/PVA semiconductor structures. *IEEE Trans. Nanotechnol.* **18**, 432–436 (2019)
 38. F. Gaâbel, M. Khelifi, N. Hamdaoui, K. Taïbi, J. Dhahri, Conduction mechanisms study CaCu_{2.8}Ni_{0.2}Ti₄O₁₂ ceramics sintered at different temperatures. *J. Alloys Compd.* **828**, 154373 (2020)
 39. M. Jebli, Ch. Rayssi, N. Hamdaoui, S. Rabaoui, J. Dhahri, M. Ben Henda, I. Shaarany, Effect of Nb-doping on the structural and electrical properties of Ba_{0.97}La_{0.02}Ti_{1-x}Nb_{4x}/5O₃ ceramics at room temperature synthesized by molten-salt method. *J. Alloys Compd.* **784**, 204–212 (2019)
 40. M. Hsini, N. Hamdaoui, S. Hcini, M. Lamjed Bouazizi, S. Zemni, L. Beji, Effect of iron doping at Mn-site on complex impedance spectroscopy properties of Nd_{0.67}Ba_{0.33}MnO₃ perovskite. *Phase Transit.* **91**(3), 316–331 (2017)
 41. S.O. Tan, Identification of the frequency and voltage-dependent dielectric characterization of metal-Zn/PVA semiconductor structures. *IEEE Trans. Nanotechnol.* **18**, 432–436 (2019)

Publisher’s Note Springer Nature remains neutral with regard to jurisdictional claims in published maps and institutional affiliations.